Electronic Supplementary Material (ESI) for Chemical Science.

Multicomponent metal-organic framework membranes for advanced functional composites

Michael S. Denny, Jr., Mark Kalaj, Kyle C. Bentz, and Seth M. Cohen

Department of Chemistry and Biochemistry, University of California, San Diego, 9500 Gilman Dr., La Jolla, CA 92093 USA.

*correspondence to: scohen@ucsd.edu

Supporting Information

Materials Synthesis

UiO-66. Zirconium(IV) chloride ($ZrCl_4$, 61 mg, 0.26 mmol) and terephthalic acid (43 mg, 0.260 mmol) were dissolved in 15 mL DMF with 0.447 mL glacial acetic acid in a 20 mL vial. The capped vial was placed in an oven and heated to 120 °C for 24 h. After cooling to room temperature, the particles were collected by centrifugation (Rotor: FO685, RPM: 6200, Time: 15 min) and washed three times with 10 mL portions of each DMF and methanol and dried under vacuum at room temperature. The procedure was repeated in parallel 10 times and all products were combined.[1]

UiO-66-NH_2. Zirconium(IV) chloride ($ZrCl_4$, 61 mg, 0.26 mmol) and 2-amino terephthalic acid (47 mg, 0.260 mmol) were dissolved in 15 mL DMF with 0.447 mL glacial acetic acid in a 20 mL vial. The capped vial was placed in an oven and heated to 120 °C for 24 h. After cooling to room temperature, the particles were collected by centrifugation (Rotor: FO685, RPM: 6200, Time: 15 mins) and washed three times with 10 mL portions of each DMF and methanol and dried under vacuum at room temperature. The procedure was repeated in parallel 10 times and all products were combined.

HKUST-1. Copper(II) nitrate hemipentahydrate ($Cu(NO_3)_2 \cdot 2.5H_2O$, 1.22 g, 5.24 mmol) and 1,3,5-benzenetricarboxylic acid (0.58 g, 2.76 mmol) were dissolved in 5 mL DMSO. This solution was then added dropwise over 15 min to 250 mL of MeOH with magnetic stirring. Stirring was continued for 15 min after complete addition. The particles were collected by centrifugation (fixed-angle rotor, 6500 rpm, 15 min), washed with 3×10 mL portions of MeOH, and dried under vacuum at room temperature.[2]

ZIF-8. Zinc(II) nitrate hexahydrate ($Zn(NO_3)_2 \cdot 6H_2O$, 0.30 g, 1.0 mmol) and 2-methylimidazole (0.66 g, 8.0 mmol) were each dissolved in 15 mL MeOH. The solutions were combined and stirred vigorously for 24 h. White ZIF-8 particles were collected by centrifugation (fixed-angle rotor, 6500 rpm, 15 min), washed with 3×10 mL portions of MeOH, and dried under vacuum at room temperature.[3]

MIL-101(Fe). Iron(III) chloride hexahydrate ($FeCl_3 \cdot 6H_2O$, 94 mg, 0.348 mmol) and terephthalic acid (58 mg, 0.348 mmol) were dissolved in 15 mL DMF. The solution was transferred to a 35 mL microwave reaction vessel and the reaction mixture was heated rapidly to 150 °C (Power = 300W) and held at 150 °C for 15 min. After cooling to room temperature, the red particles were collected by centrifugation (fixed-angle rotor, 6500 rpm, 15 min), washed with 3×10 mL portions of each DMF and EtOH, and dried under vacuum at room temperature.[4]

MIL-53(Fe). Iron(III) chloride hexahydrate ($FeCl_3 \cdot 6H_2O$, 0.540 g, 2 mmol) and terephthalic acid (332 mg, 2 mmol) were dissolved in 10 mL DMF. The solution was transferred to a Teflon lined stainless steel Parr bomb and heated to 150 °C (temperature ramped over 1 h, 2.5 °C/min) and held at temperature for 15 h. After cooling to room temperature, the yellow product was collected by centrifugation (fixed-angle rotor, 6500 rpm, 15 min), washed with 3×10 mL portions of each DMF and EtOH, and dried under vacuum at room temperature.[5]

MIL-101-NO_2. Chromium (VI) oxide (CrO_3, 1.25 g, 12.5 mmol), 2-nitroterephthalic acid (2.64 g, 12.5 mmol), and 12 M HCl (1.8 g, 50 mmol) were dissolved in 50 mL water. The solution was transferred to a Teflon lined stainless steel Parr bomb and heated to 180 °C and held at temperature

for 6 days. After cooling to room temperature, the green product was collected by centrifugation (fixed-angle rotor, 6500 rpm, 15 min), washed with 3×400 mL portions of water, then with 3 x 100 mL of MeOH, and dried under vacuum at room temperature.[6]

MOF MMM Fabrication

General Information. Starting materials and solvents were purchased and used without further purification from commercial suppliers (Sigma-Aldrich, Alfa Aesar, EMD, TCI, and others). PVDF (Kynar HSV-900) was kindly provided by Arkema. Details of MOF syntheses and postsynthetic protocols are provided in the Electronic Supporting Information (ESI).

MOF MMM ink formulation. Single MOF inks were prepared according to the literature procedure.[7] In a typical MOF ink preparation for a 60% wt. MMM, 120 mg of MOF was dispersed in 5 mL acetone with sonication for 30 mins in a scintillation vial. 1.07 g of a PVDF solution (7.5% wt. in DMF) was then added to the MOF suspension. The suspension was further sonicated for 30 min and then the acetone was removed by rotary evaporation, resulting in the final MOF 'ink'.

This same procedure was adapted for multiple MOF species. For example, to prepare an ink for a 60% MOF MMM containing UiO-66 and HKUST-1 in equal ratios, 60 mg UiO-66 and 60 mg HKUST-1 are dispersed together in 5 mL acetone, then treated as above. MOF ratios in the final product may be adjusted by adjusting the composition of the ink.

Crosslinked MMM ink formulation. Inks for crosslinked MOF MMMs were prepared by following the same procedure as above. Then, after removal of the acetone by rotary evaporation, 1,6-hexamethylene diamine (HMDA) was added to the ink formulation at 5 mol % relative to the PVDF monomer in the ink. For example, in the ink for preparing a 60% wt. MMM described above, 8.5 μL HMDA was added to the MOF ink. The ink with HMDA added was then sonicated for 30 min to ensure homogeneity of the ink.

MOF MMM fabrication. Films were cast from these MOF inks on Al foil substrates by drawdown coating using a 400 μm doctor blade at a coating speed of 25 mm/s. The films were then heated to remove solvent (1 h in an oven at 70 °C, or 12 h at 100 °C for crosslinked MMMs). The MMMs were then delaminated from the Al substrate by immersion in CH_3OH. The resulting free-standing films were dried in air prior to characterization and use.

Materials Characterization

Powder X-Ray Diffraction (PXRD). ~50 mg of MOF powder or a 1 cm^2 piece of MOF MMM was mounted on a silicon sample holder for analysis by PXRD. PXRD data were collected at ambient temperature on a Bruker D8 Advance diffractometer at 40 kV, 40 mA for Cu Kα radiation (λ = 1.5418 Å), with a scan speed of 2 sec/step, a step size of 0.02° in 2θ, and a 2θ range of 4-50°.

Surface Area Analysis. Samples for analysis were evacuated on a vacuum line overnight at room temperature prior to analysis. ~50 mg of MOF powder or MOF MMM were then transferred to

pre-weighed sample tubes and degassed at 105 °C on a Micromeritics ASAP 2020 Adsorption Analyzer for a minimum of 12 h or until the outgas rate was <5 mmHg. After degassing, the sample tubes were re-weighed to obtain a consistent mass for the samples. Sorption data and Brunauer-Emmett-Teller (BET) surface area (m^2/g) measurements were collected at 77 K with N_2 on a Micromeritics ASAP 2020 Adsorption Analyzer using the volumetric technique.

Scanning Electron Microscopy (SEM-EDX). MOF powders and MMMs were adhered to conductive carbon tape on a sample holder disk, and coated using a Ir-sputter coating for 9 sec. A FEI Quanta FEG 250 ESEM instrument was used for acquiring images using a 10 kV energy source under vacuum at a working distance at 10 mm. Energy dispersive X-ray spectroscopy (EDX) spectra were obtained for the samples via the attached Thermo Scientific Pathfinder EDX system.

Nuclear Magnetic Resonance Spectroscopy (NMR). Proton nuclear magnetic resonance spectra (^{1}H NMR) were recorded on a Varian FT-NMR spectrometer (400 MHz). Chemical shifts are quoted in parts per million (ppm) referenced to the appropriate solvent peak or 0 ppm for TMS.

Contact angle measurements. Water contact angles were measured using a a Ramé-Hart DROPimage CA v2.5 instrument and the manufacturer's software.

Dynamic Mechanical Analysis. Dynamic mechanical analysis (DMA) was performed on a Perkin Elmer DMA 8000 (Waltham, MA). Frequency sweeps were performed at 25 °C, 0.1 to 10 Hz, and 10 μm strain on rectangular sample films approximately 12 mm by 4 mm and 50 μm in thickness. All samples were run in triplicate and data points represent an average of all runs, with error bars given as 1 standard deviation.

The dynamic elastic modulus, also known as storage modulus, *E*', is a quantity that describes the resistance of a material to elastic deformation, or more generally is related to the stiffness of a material. Application of a sinusoidal stress, σ, to a material results in a sinusoidal strain response, ε, shifted by a quantity δ, known as the phase angle. The ratio of the applied stress to strain response gives the complex modulus, *E**. Finally, the storage modulus at any particular frequency, ω, is given by

$$E'(\omega) = |E^*| \cdot \cos\delta$$

where $\cos\delta$ represents the real, in-phase, component of the strain response.

Supporting Figures

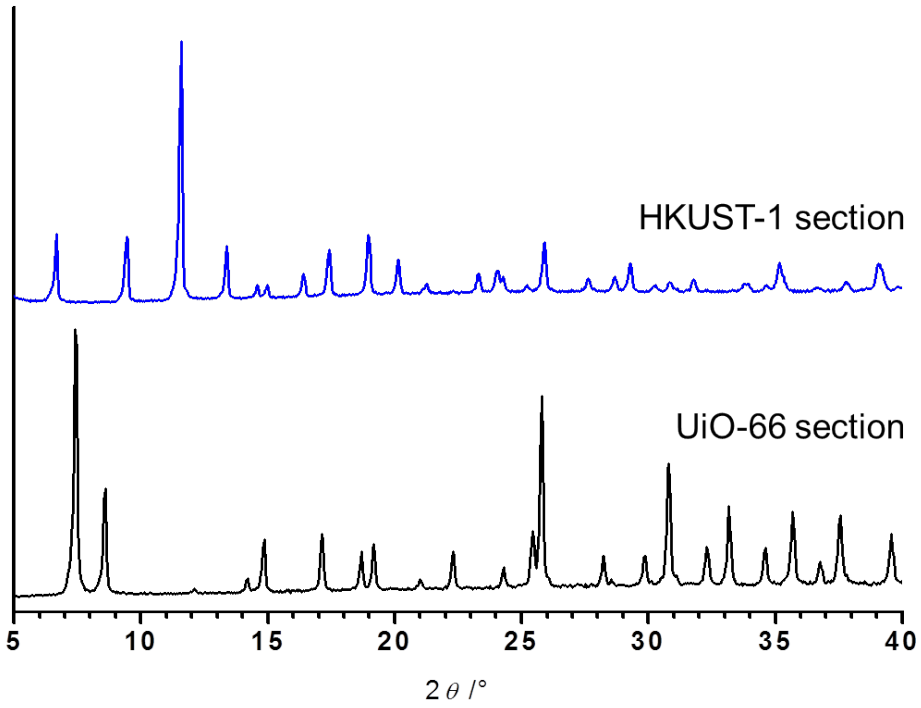

Figure S1. PXRD spectra of different areas of co-cast MMM. The black trace shows the spectrum from the UiO-66 area of the MMM and the blue trace shows the spectrum from the HKUST-1 area of the film.

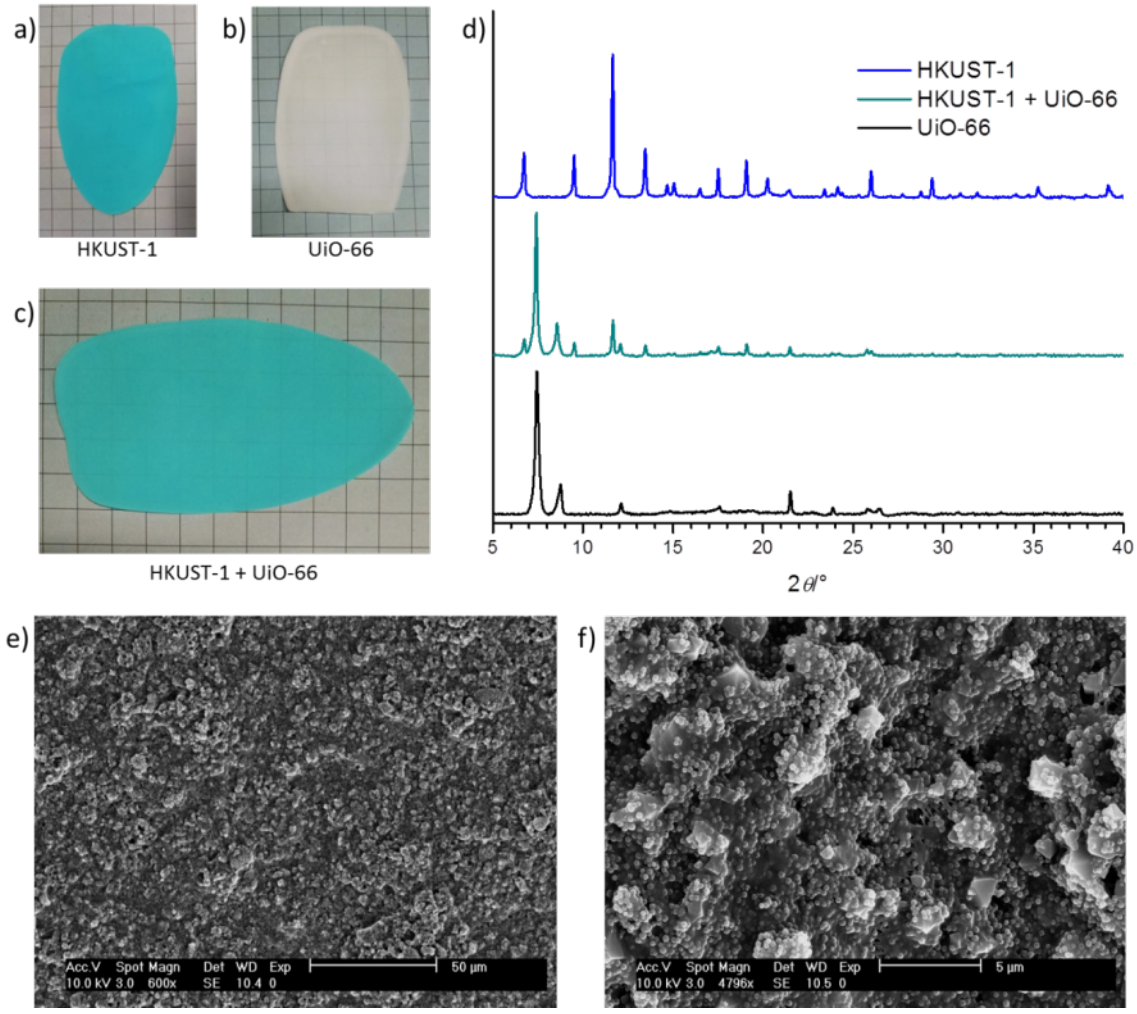

Figure S2. a) 60% wt. HKUST-1 MMM. b) 60% wt. UiO-66 MMM. c) 60% wt. HKUST-1 + UiO-66 MMM. d) PXRD spectra for each MMM. e, f) SEM images of the HKUST-1 + UiO-66 MMM. The large particles are HKUST-1 and the small particles are UiO-66.

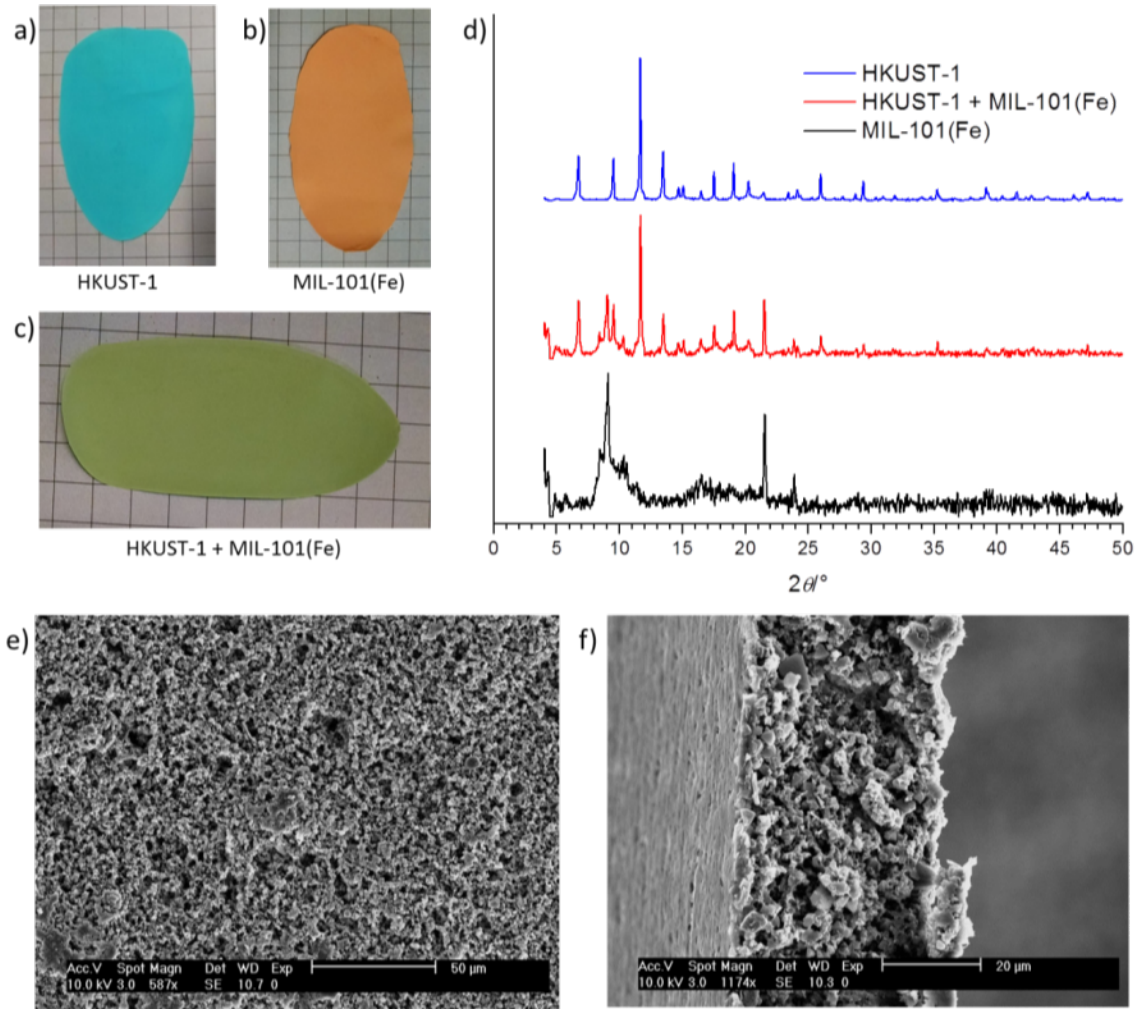

Figure S3. a) 60% wt. HKUST-1 MMM. b) 60% wt. MIL-101(Fe) MMM. c) 60% wt. HKUST-1 + MIL-101(Fe) MMM. d) PXRD spectra for each MMM. e) Plan-view and f) cross section SEM images of the HKUST-1 + MIL-101(Fe) MMM. The large particles are HKUST-1 and the small particles are MIL-101(Fe).

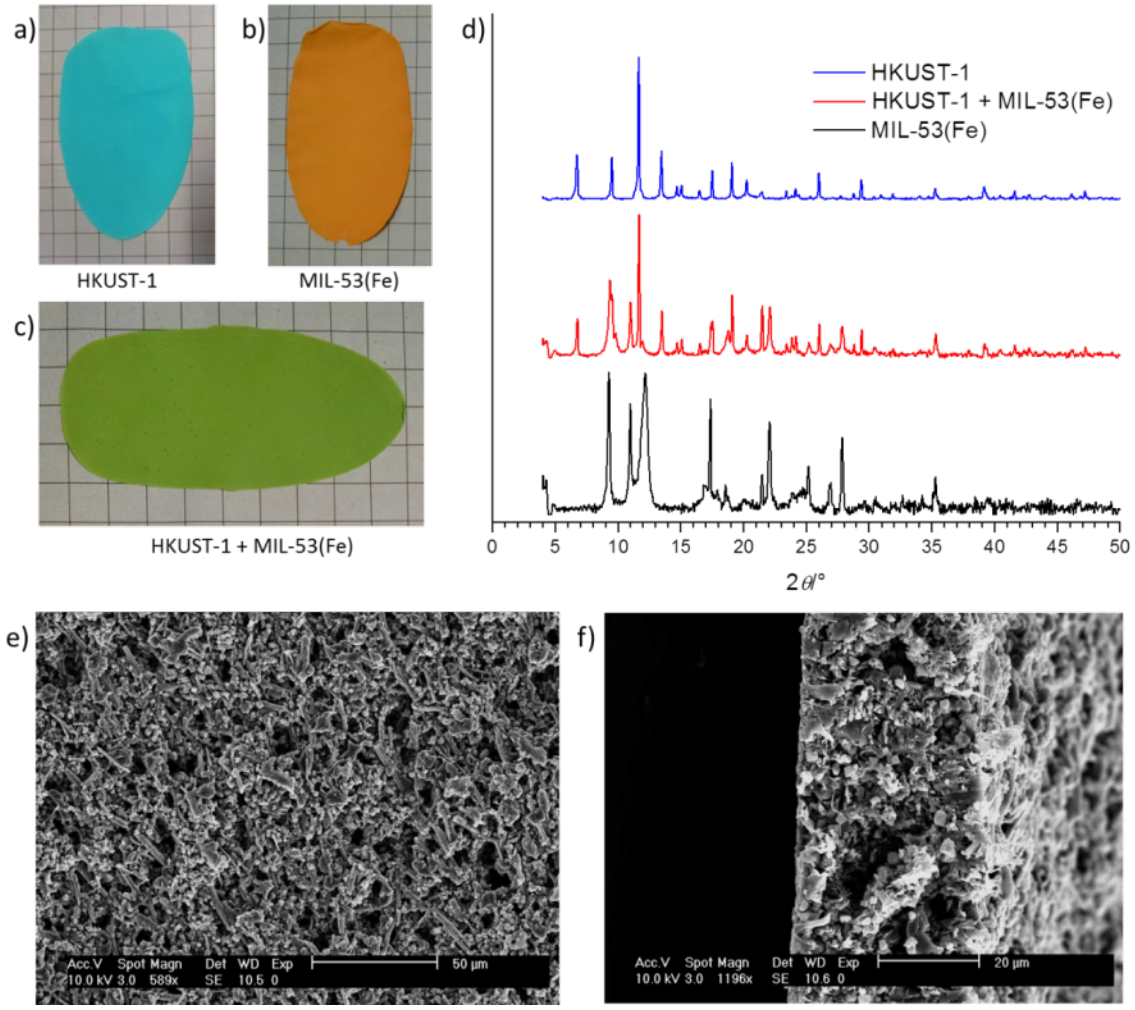

Figure S4. a) 60% wt. HKUST-1 MMM. b) 60% wt. MIL-53(Fe) MMM. c) 60% wt. HKUST-1 + MIL-53(Fe) MMM. d) PXRD spectra for each MMM. e) Plan-view and f) cross section SEM images of the HKUST-1 + MIL-53(Fe) MMM. The large, anisotropic particles are MIL-53(Fe) and the smaller, octahedral particles are HKUST-1.

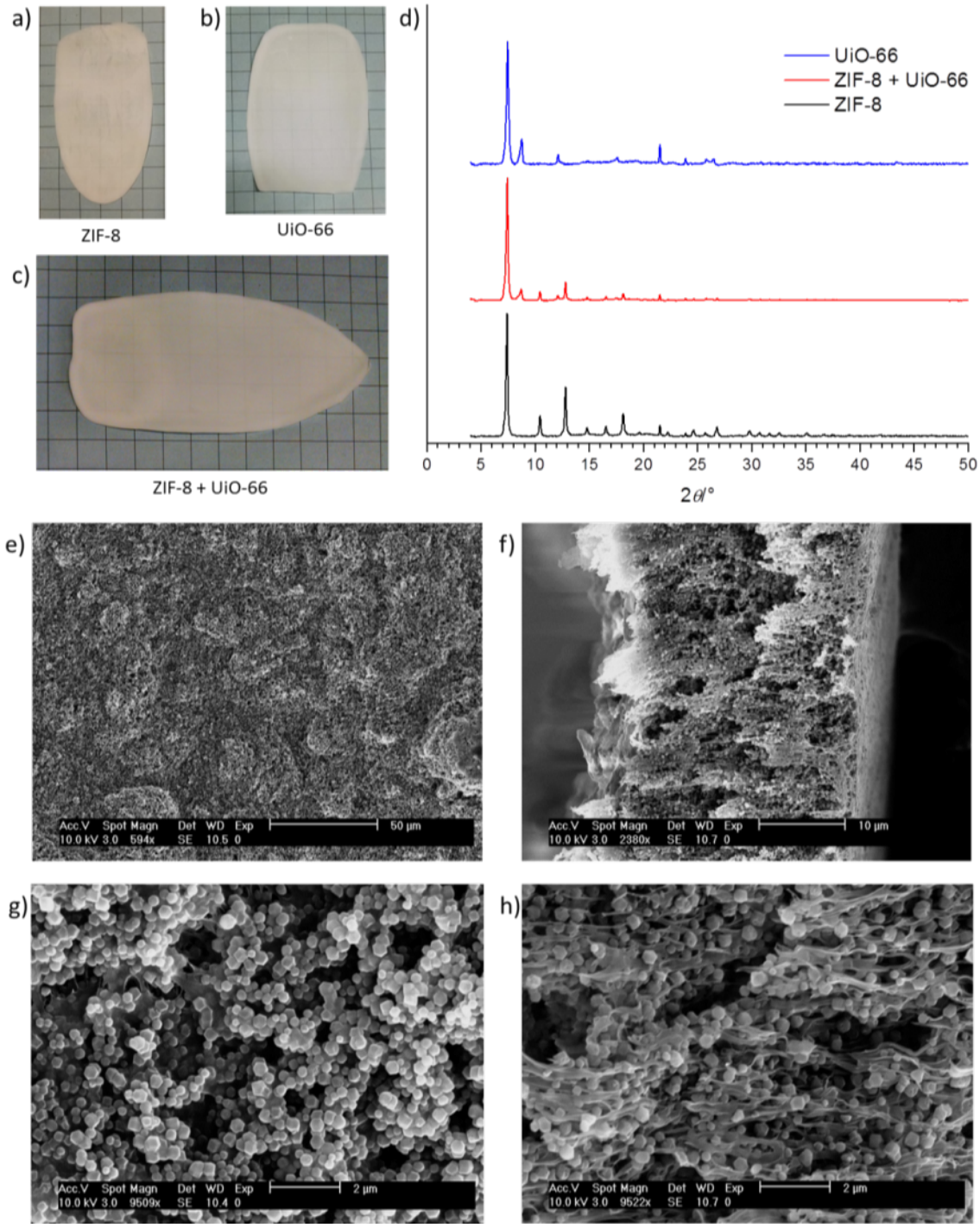

Figure S5. a) 60% wt. ZIF-8 MMM. b) 60% wt. UiO-66 MMM. c) 60% wt. ZIF-8 + UiO-66 MMM. d) PXRD spectra for each MMM. e, g) Plan-view and f, h) cross section SEM images of the ZIF-8 + UiO-66 MMM.

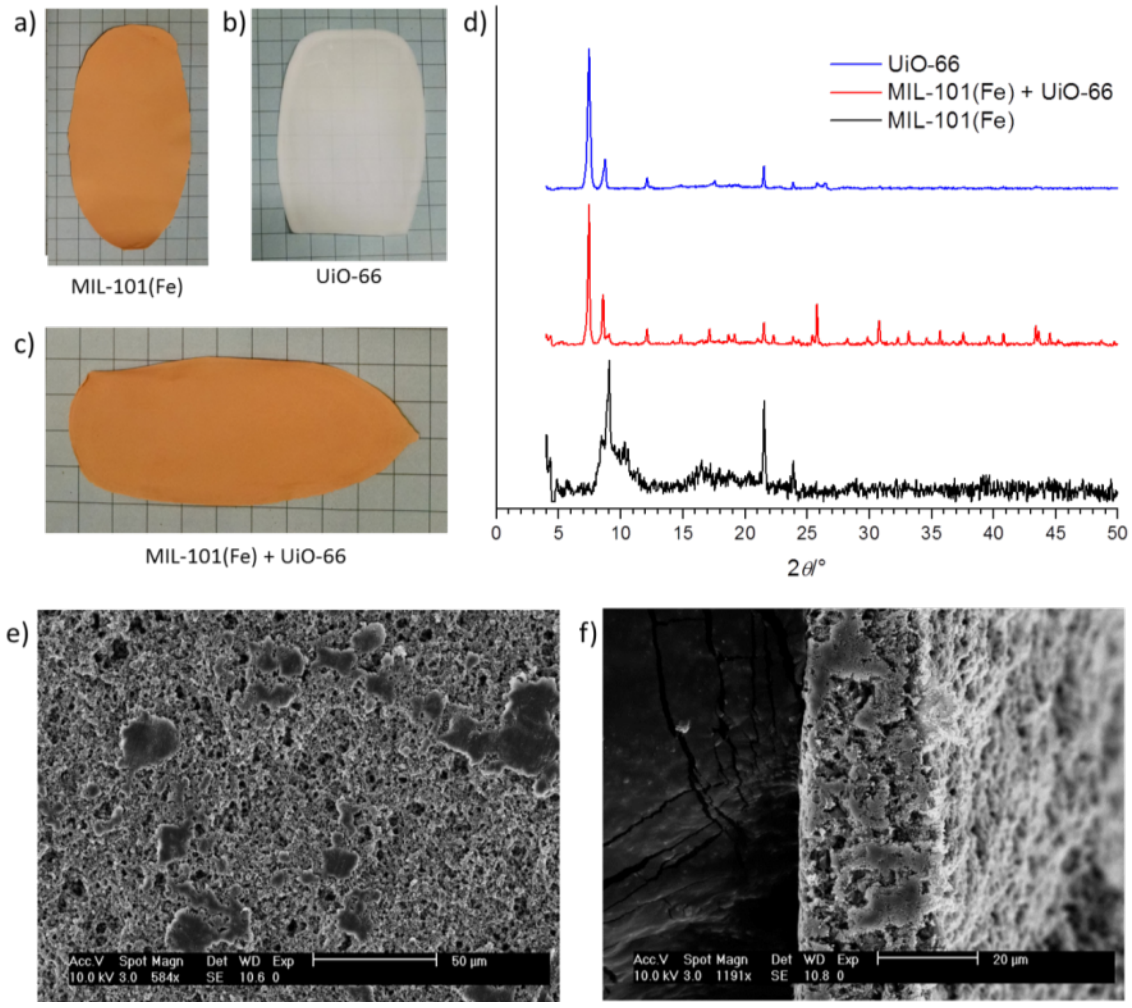

Figure S6. a) 60% wt. MIL-101(Fe) MMM. b) 60% wt. UiO-66 MMM. c) 60% wt. MIL-101(Fe) + UiO-66 MMM. d) PXRD spectra for each MMM. e) Plan-view and f) cross section SEM images of the ZIF-8 + UiO-66 MMM.

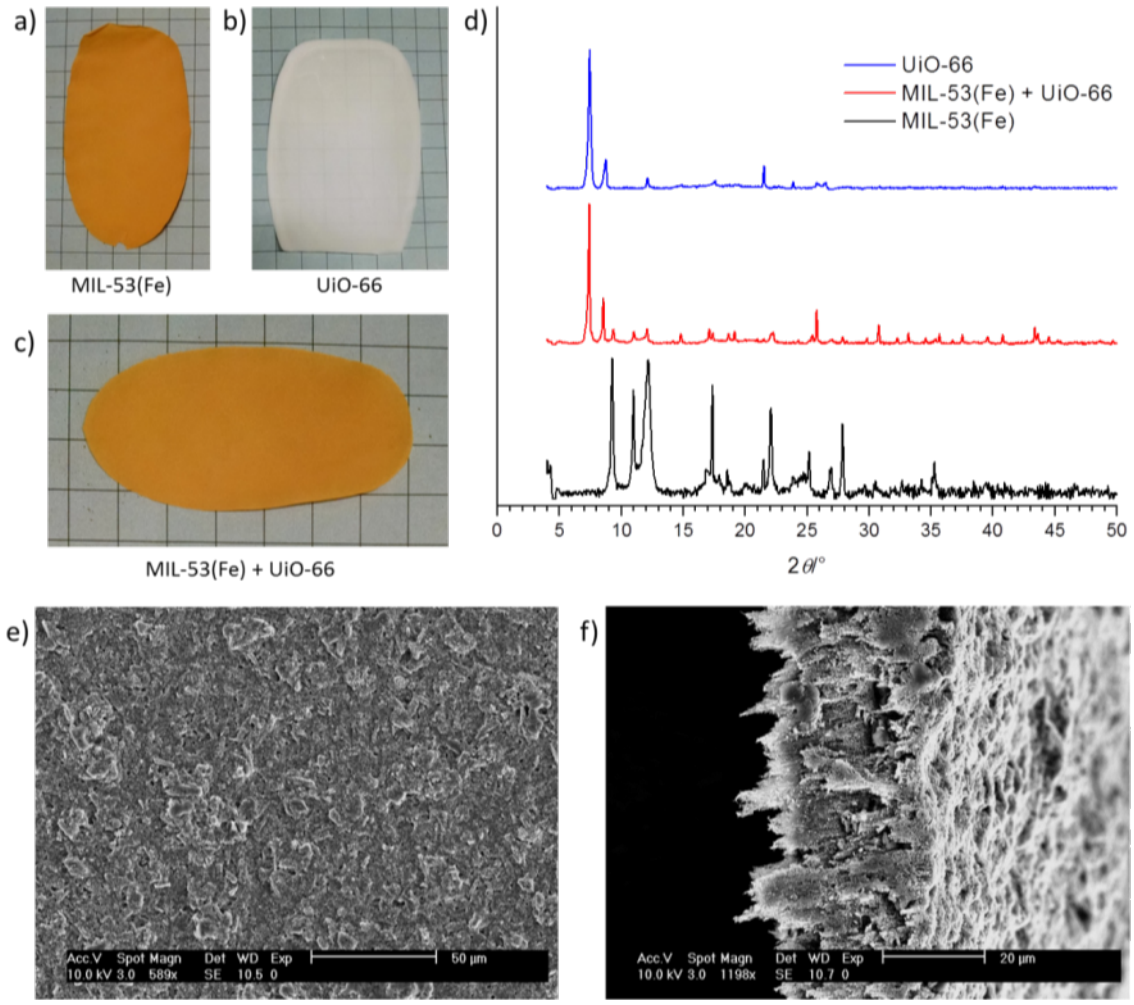

Figure S7. a) 60% wt. MIL-53(Fe) MMM. b) 60% wt. UiO-66 MMM. c) 60% wt. MIL-53(Fe) + UiO-66 MMM. d) PXRD spectra for each MMM. e) Plan-view and f) cross section SEM images of the MIL-53(Fe) + UiO-66 MMM. The large particles are MIL-53(Fe) and the small particles are UiO-66.

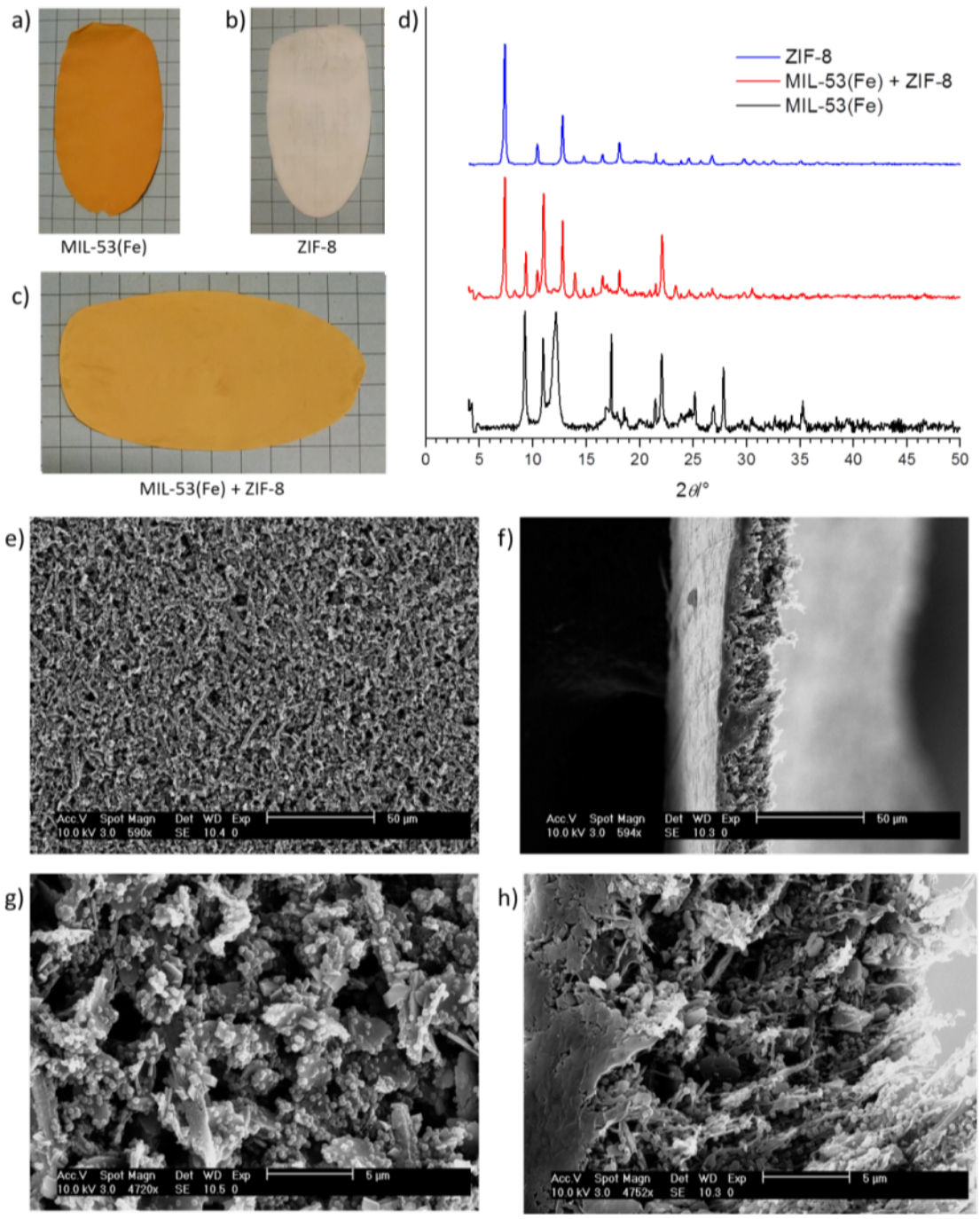

Figure S8. a) 60% wt. MIL-53(Fe) MMM. b) 60% wt. ZIF-8 MMM. c) 60% wt. MIL-53(Fe) + ZIF-8 MMM. d) PXRD spectra for each MMM. e) Plan-view and f) cross section SEM images of the MIL-53(Fe) + ZIF-8 MMM. The large particles are MIL-53(Fe) and the small particles are ZIF-8.

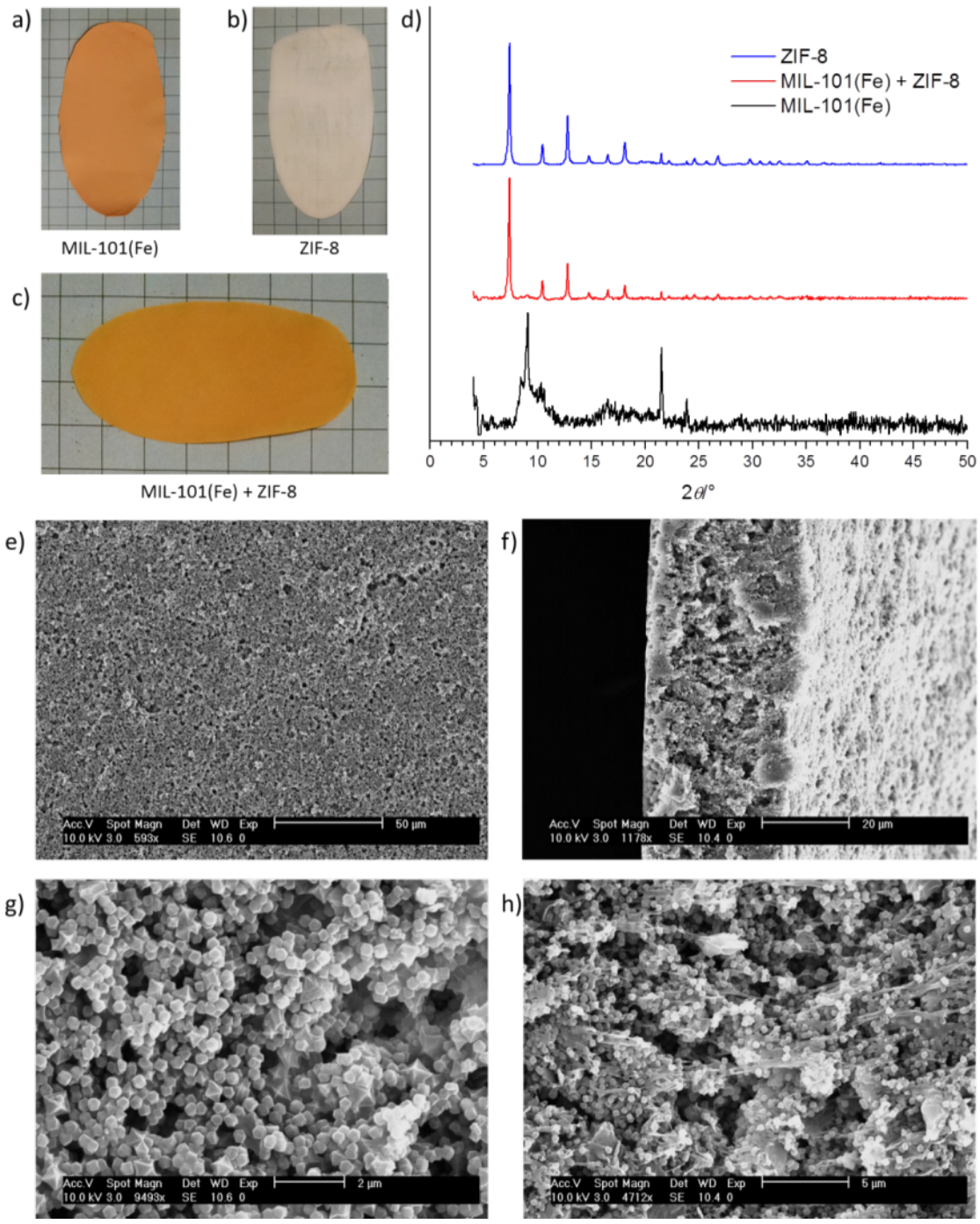

Figure S9. a) 60% wt. MIL-101 (Fe) MMM. b) 60% wt. ZIF-8 MMM. c) 60% wt. MIL-101(Fe) + ZIF-8 MMM. d) PXRD spectra for each MMM. e, g) Plan-view and f, h) cross section SEM images of the MIL-101(Fe) + ZIF-8 MMM. The octahedral particles are MIL-101(Fe) and the small particles are ZIF-8.

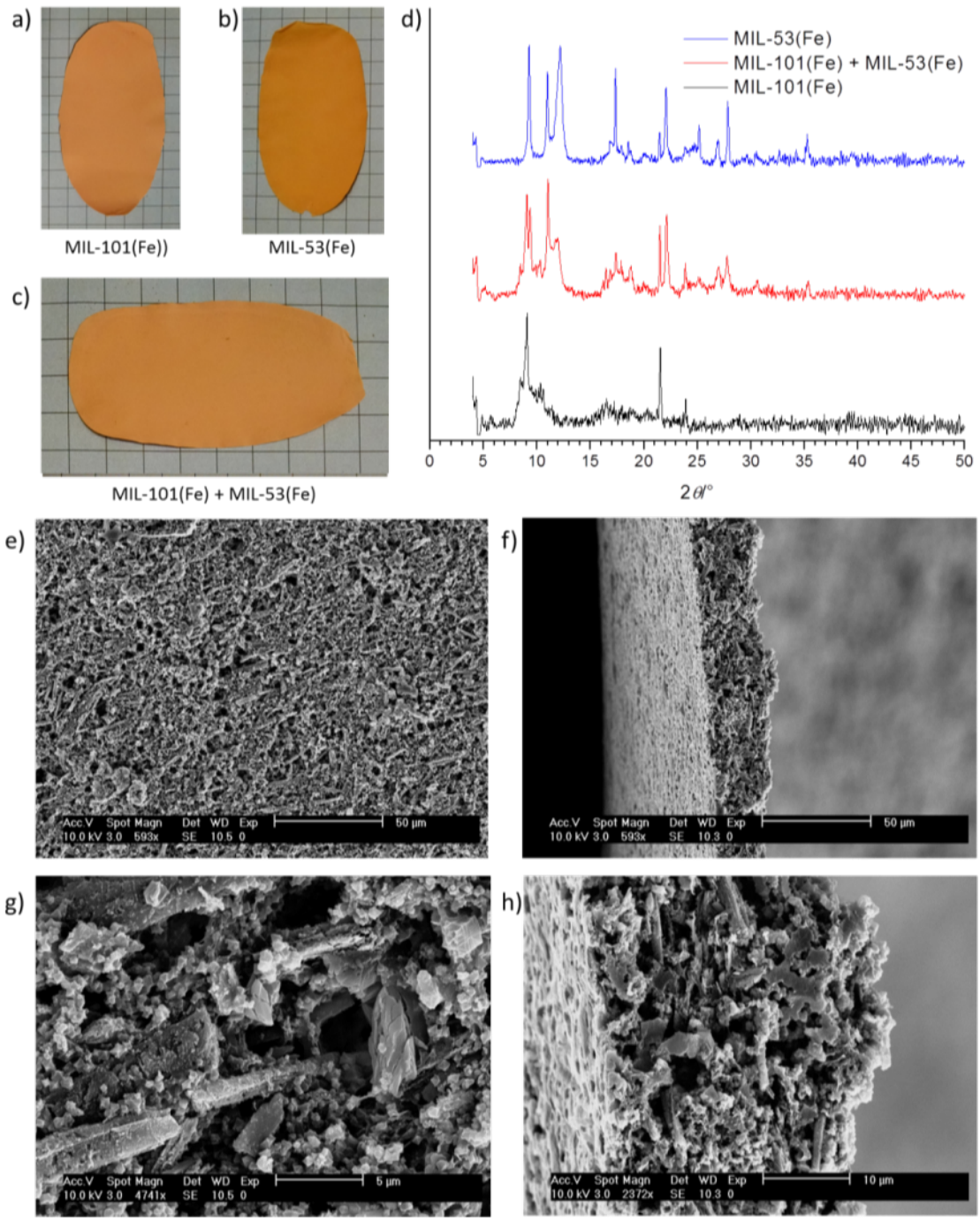

Figure S10. a) 60% wt. MIL-101 (Fe) MMM. b) 60% wt. MIL-53(Fe) MMM. c) 60% wt. MIL-101(Fe) + MIL-53(Fe) MMM. d) PXRD spectra for each MMM. e, g) Plan-view and f, h) cross section SEM images of the MIL-101(Fe) + MIL-53 MMM. The large particles are MIL-53(Fe) and the small particles are MIL-101(Fe).

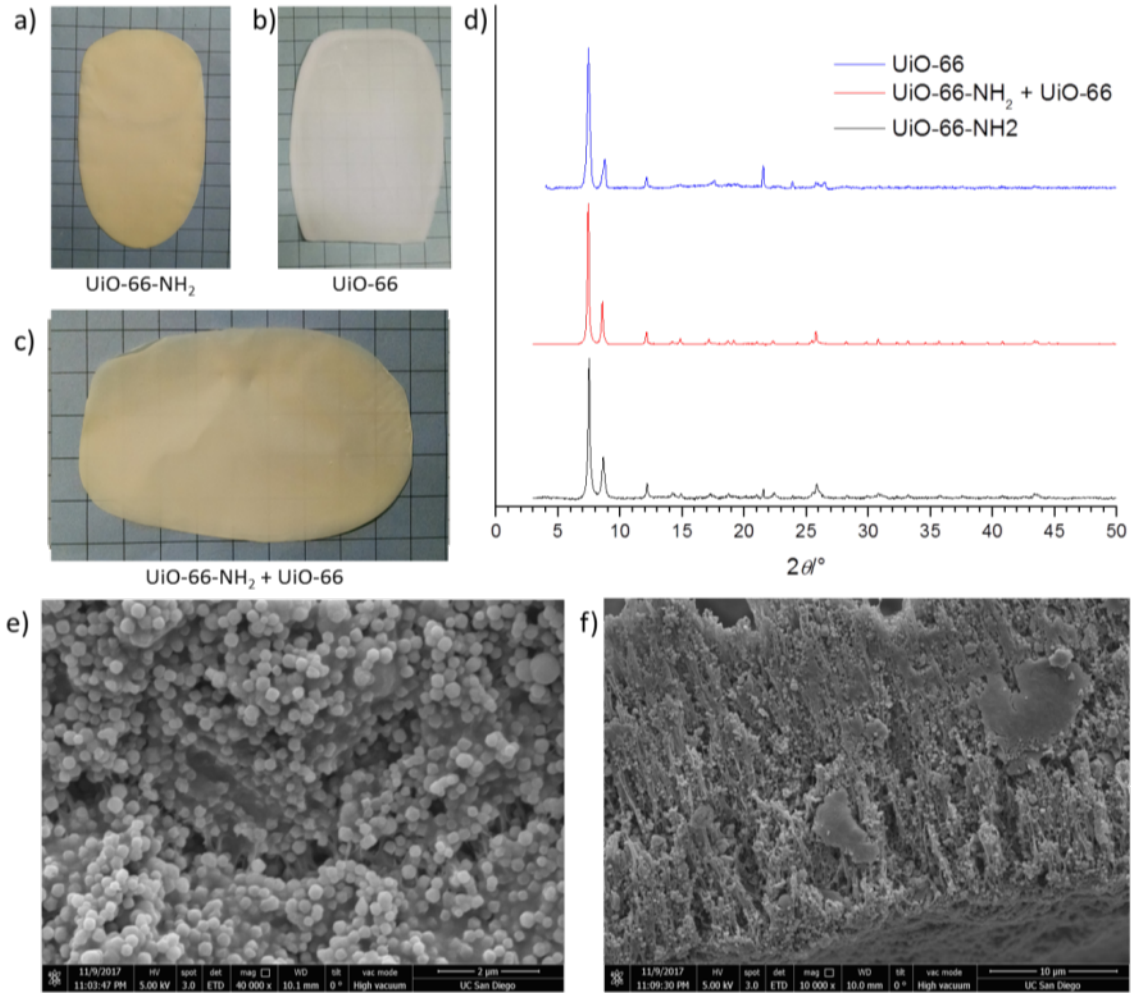

Figure S11. a) 60% wt. UiO-66-NH_2 MMM. b) 60% wt. UiO-66 MMM. c) 60% wt. UiO-66-NH_2 + UiO-66 MMM. d) PXRD spectra for each MMM. e) Plan-view and f) cross section SEM images of the UiO-66-NH_2 + UiO-66 MMM.

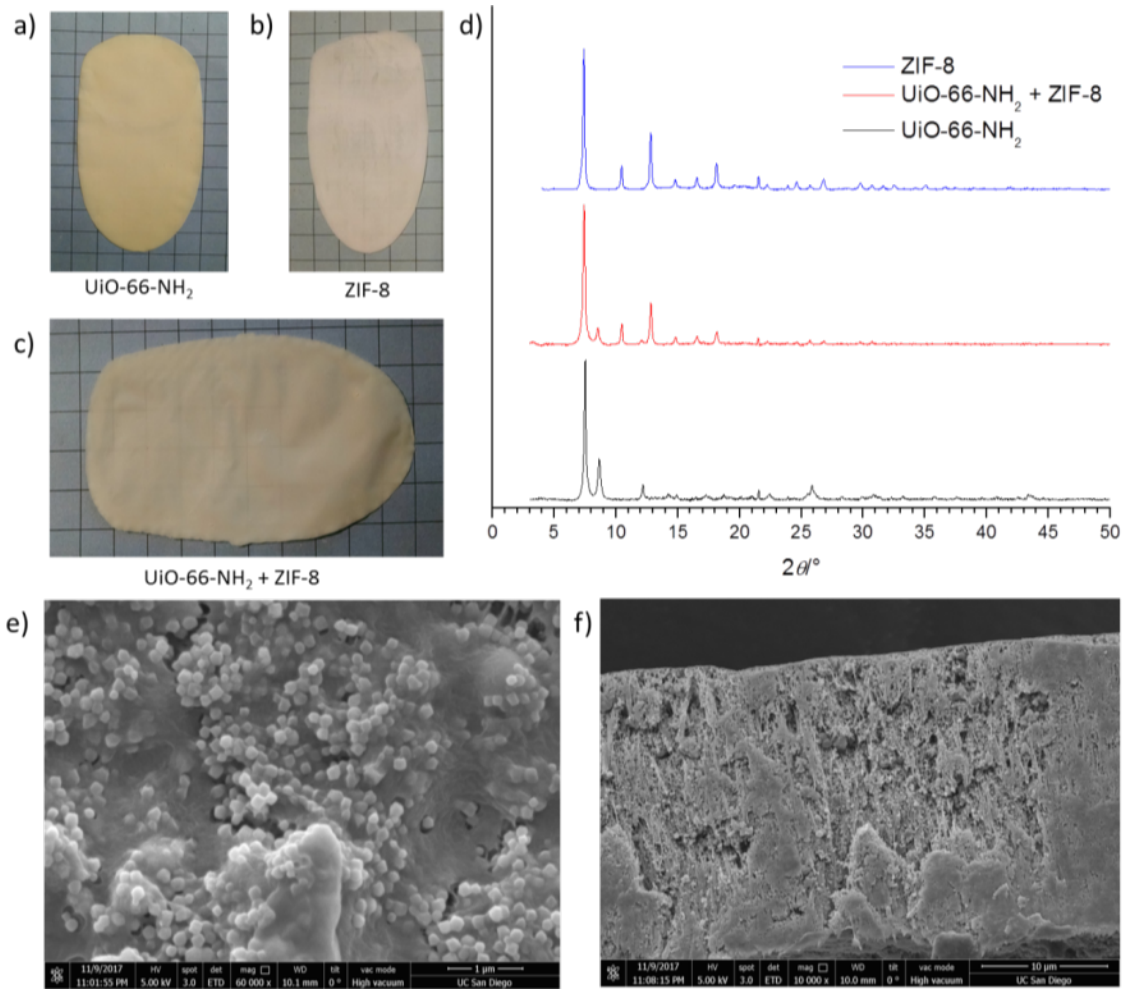

Figure S12. a) 60% wt. UiO-66-NH_2 MMM. b) 60% wt. ZIF-8 MMM. c) 60% wt. UiO-66-NH_2 + ZIF-8 MMM. d) PXRD spectra for each MMM. e) Plan-view and f) cross section SEM images of the UiO-66-NH_2 + ZIF-8 MMM.

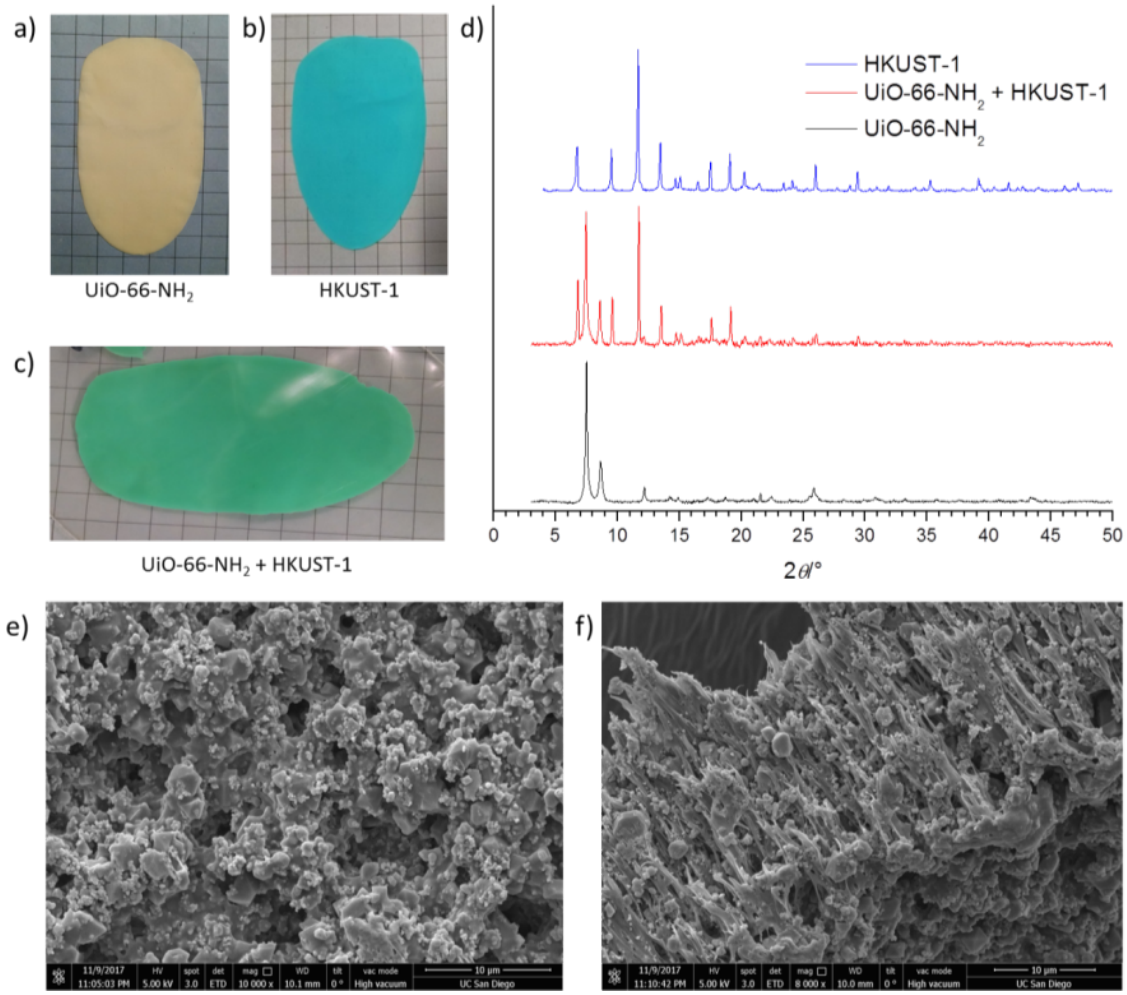

Figure S13. a) 60% wt. UiO-66-NH_2 MMM. b) 60% wt. HKUST-1 MMM. c) 60% wt. UiO-66-NH_2 + HKUST-1 MMM. d) PXRD spectra for each MMM. e) Plan-view and f) cross section SEM images of the UiO-66-NH_2 + HKUST-1 MMM.

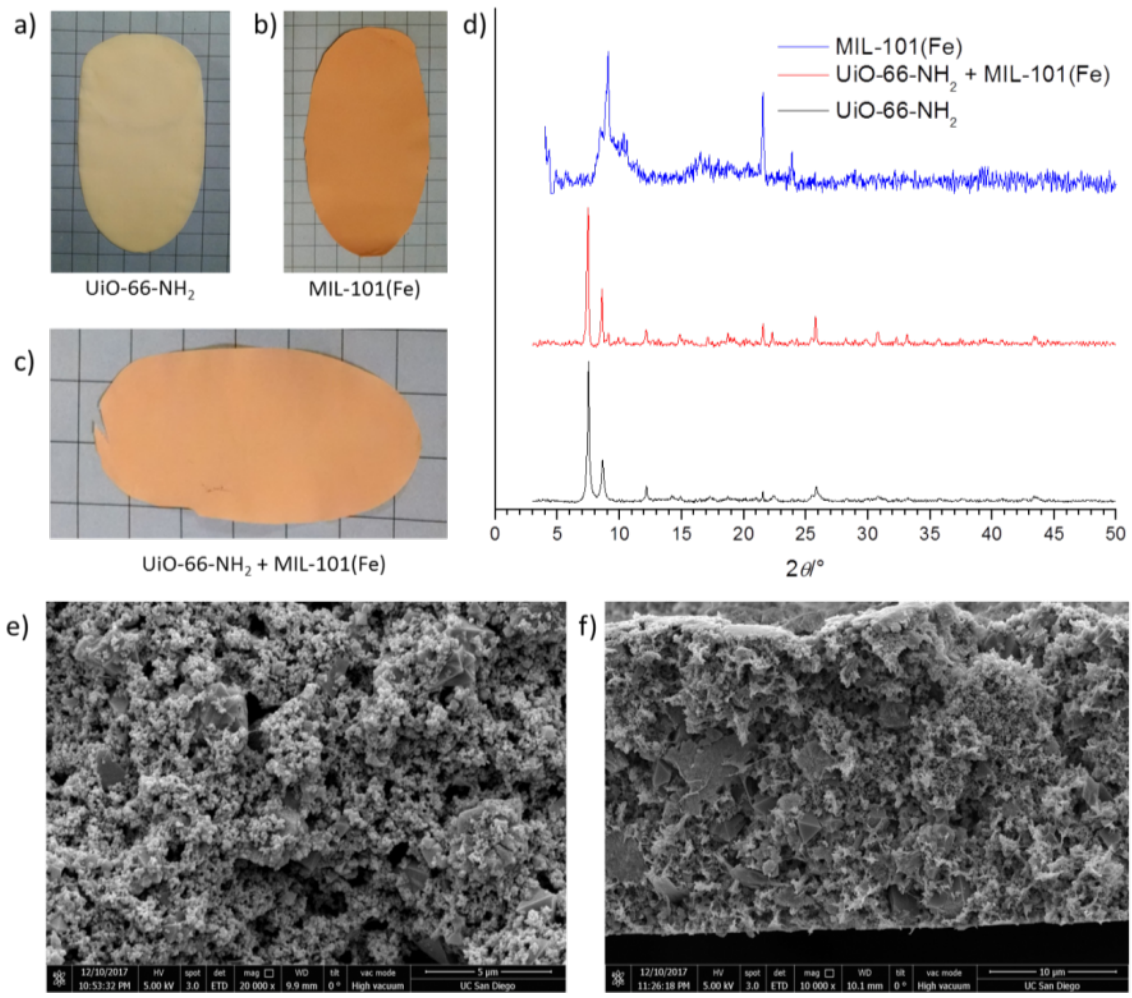

Figure S14. a) 60% wt. UiO-66-NH_2 MMM. b) 60% wt. MIL-101(Fe) MMM. c) 60% wt. UiO-66-NH_2 + MIL-101(Fe) MMM. d) PXRD spectra for each MMM. e) Plan-view and f) cross section SEM images of the UiO-66-NH_2 + MIL-101(Fe) MMM.

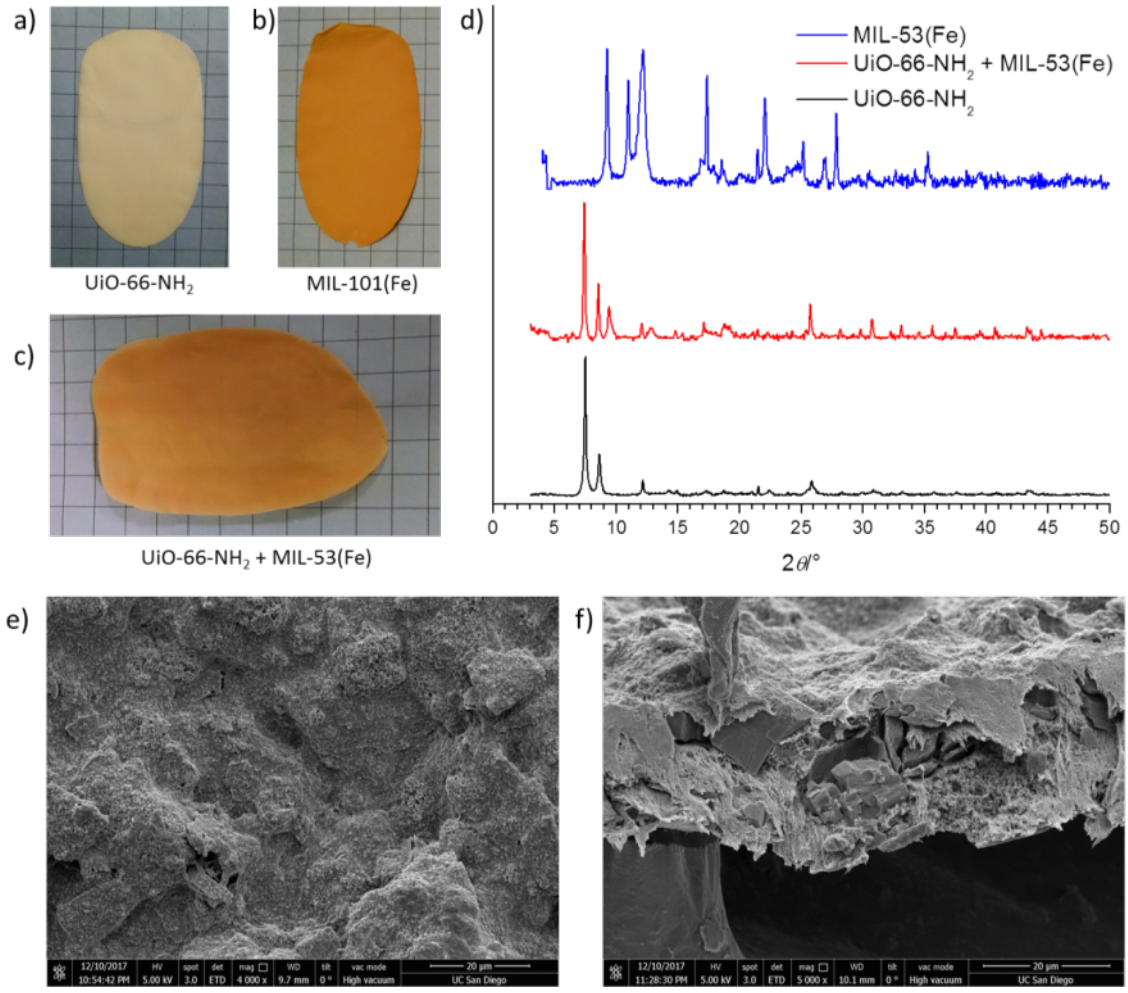

Figure S15. a) 60% wt. UiO-66-NH_2 MMM. b) 60% wt. MIL-53(Fe) MMM. c) 60% wt. UiO-66-NH_2 + MIL-53(Fe) MMM. d) PXRD spectra for each MMM. e) Plan-view and f) cross section SEM images of the UiO-66-NH_2 + MIL-53(Fe) MMM.

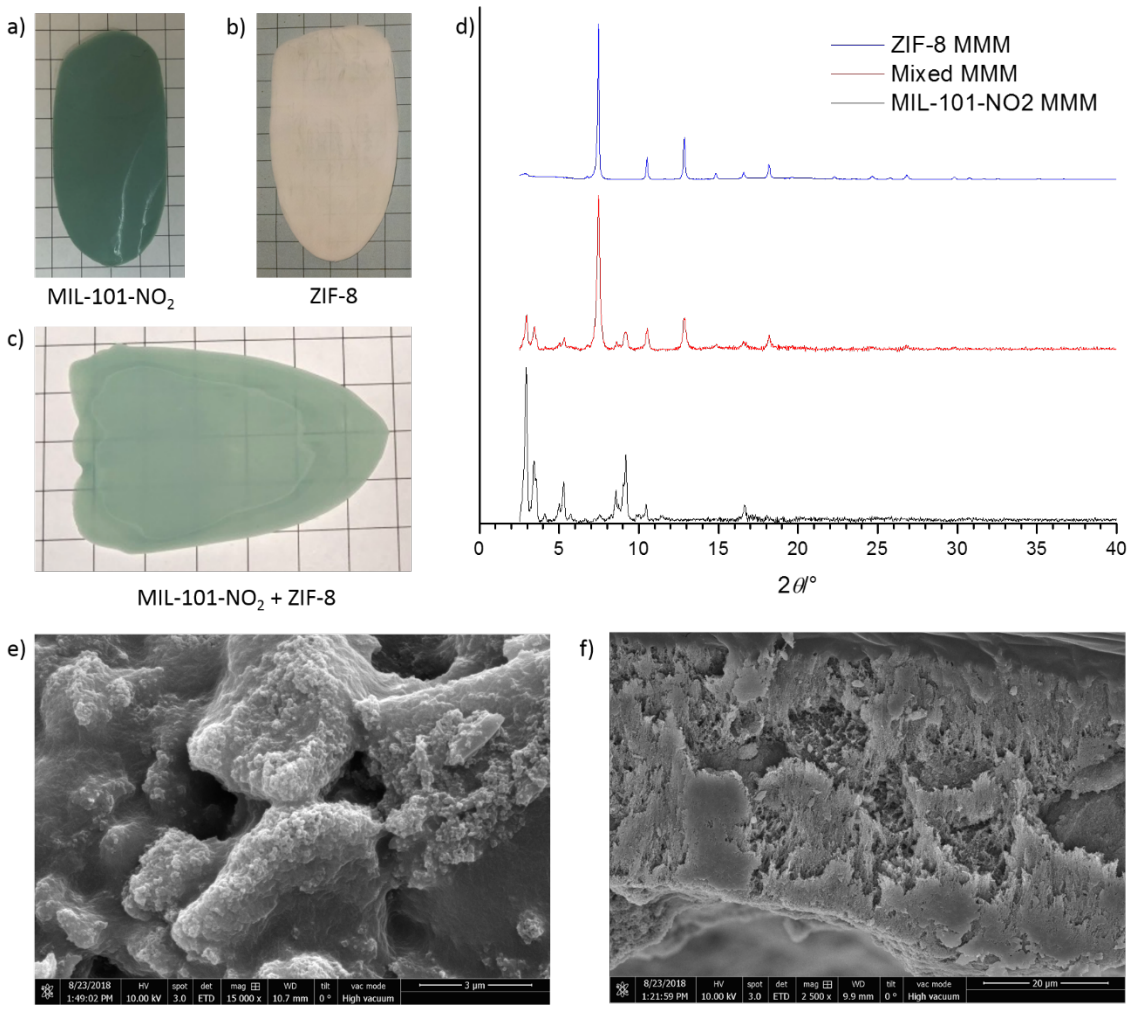

Figure S16. a) 60% wt. MIL-101-NO_2 MMM. b) 60% wt. ZIF-8 MMM. c) 60% wt. MIL-101-NO_2 + ZIF-8 MMM. d) PXRD spectra for each MMM. e) Plan-view and f) cross section SEM images of the 60% wt. MIL-101-NO_2 + ZIF-8 MMM.

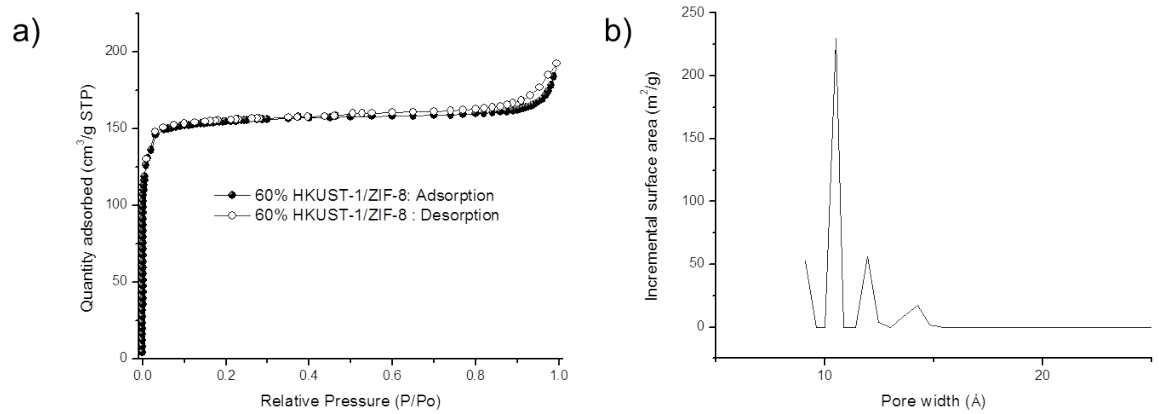

Figure S17. a) N_2 sorption isotherm of the mixed HKUST-1 + ZIF-8 MMM (60% wt.) BET surface area = 635 m^2/g, which scaled well to the amount of MOF in the MMM, indicating that the MOF pores remain accessible in the composite. b) The pore width distribution (N_2 DFT) also corresponds well to the 11 Å pores of the ZIF-8 and the three different pore sizes of the HKUST-1 (9.5 Å, 12 Å, and 13.3 Å).

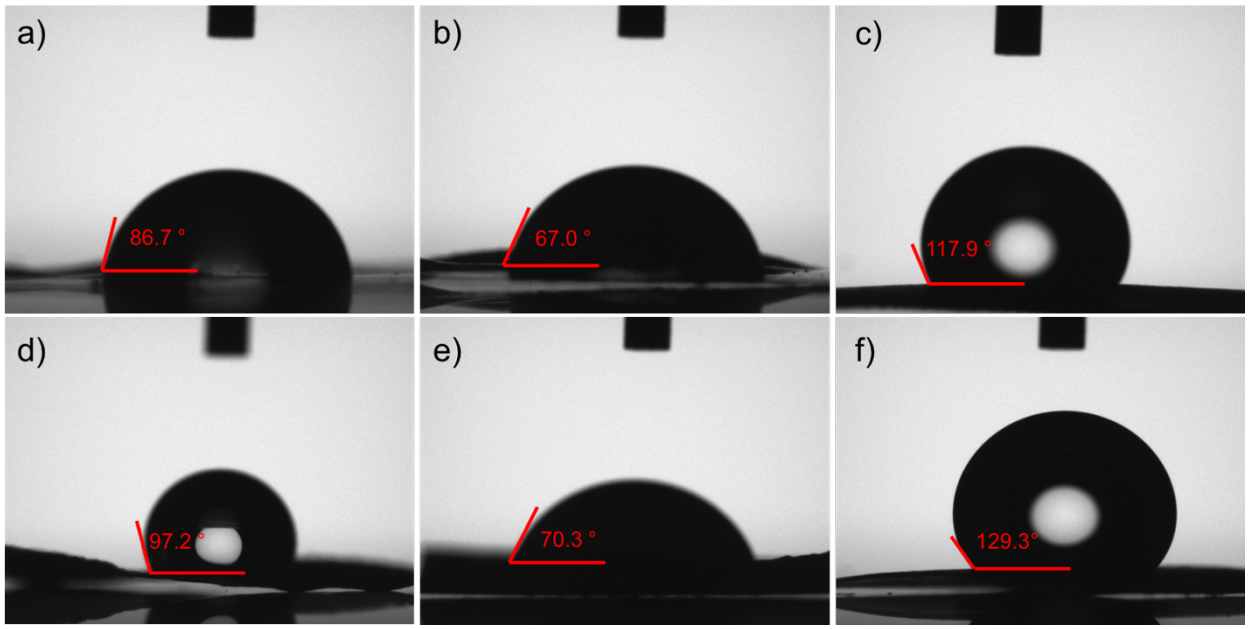

Figure S18. Water contact angles and images measured on various MMMs: a) PVDF, b) 67% ZIF-8 MMM, c) 67% HKUST-1 MMM, d) Mixed MOF (ZIF-8/HKUST-1) MMM, e) Layered MMM (ZIF-8 side) f) Layered MMM (HKUST-1 side). The differences in measured contact angles for all samples were not statistically significant (n=3).

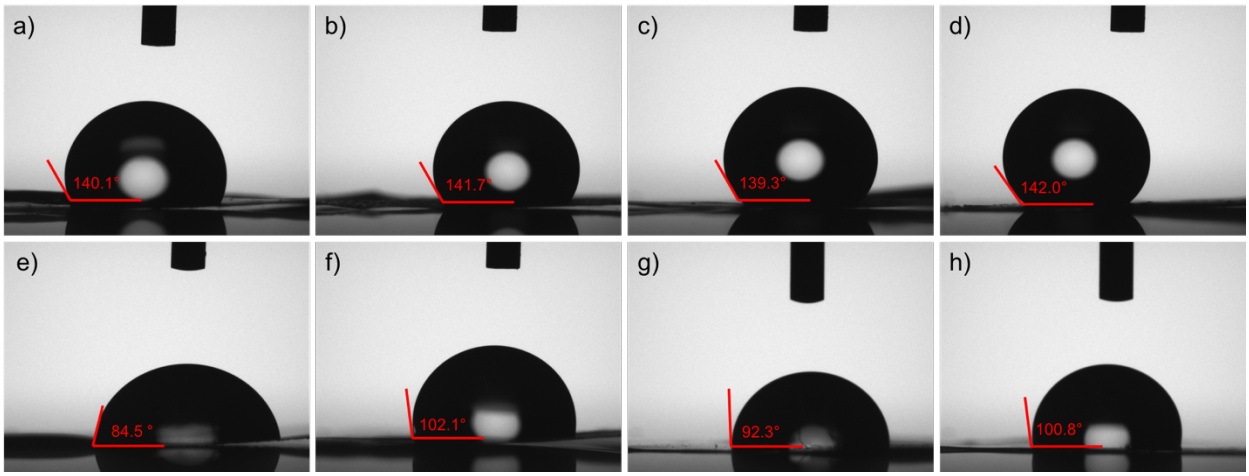

Figure S19. Water contact angles and images measured on various MMMs: a) 67% UiO-66-NH2 MMM, b) 67% UiO-66 MMM, c) 67% MIL-53(Fe) MMM, d) 67% MIL-101(Fe) MMM, e) MMM Mixed MOF (ZIF-8/UiO-66-NH2) f) MMM Mixed MOF (ZIF-8/UiO-66) g) MMM Mixed MOF (ZIF-8/MIL-53(Fe)) h) MMM Mixed MOF (ZIF-8/MIL-101(Fe)). The differences in measured contact angles for all samples were not statistically significant (n=3).

Dynamic Mechanical Analysis. All materials displayed an expected frequency independent response of modulus over the frequency range probed at ambient temperature conditions, as shown in Figure 1. The pure PVDF polymer film had a modulus (*E*') of 215 ± 6 MPa, with enhancement of the moduli with the introduction of inorganic fillers, as is commonly observed in polymer nanocomposite films.[8,9] Introduction of ZIF-8 into PVDF films at 67 wt% resulted in qualitatively brittle samples, and only a modest increase in modulus was observed, with a value of 257 ± 40. HKUST-1 MMMs were comparatively much more pliable, and quantitatively, much more robust than ZIF-8 MMMs, with a modulus of 519 ± 10. Mixed and layered MMMs with equal quantities of ZIF-8 and HKUST-1 resulted in materials with comparable moduli to HKUST-1 MMMs, with values of 549 ± 117 and 424 ± 28, respectively (Table 1).

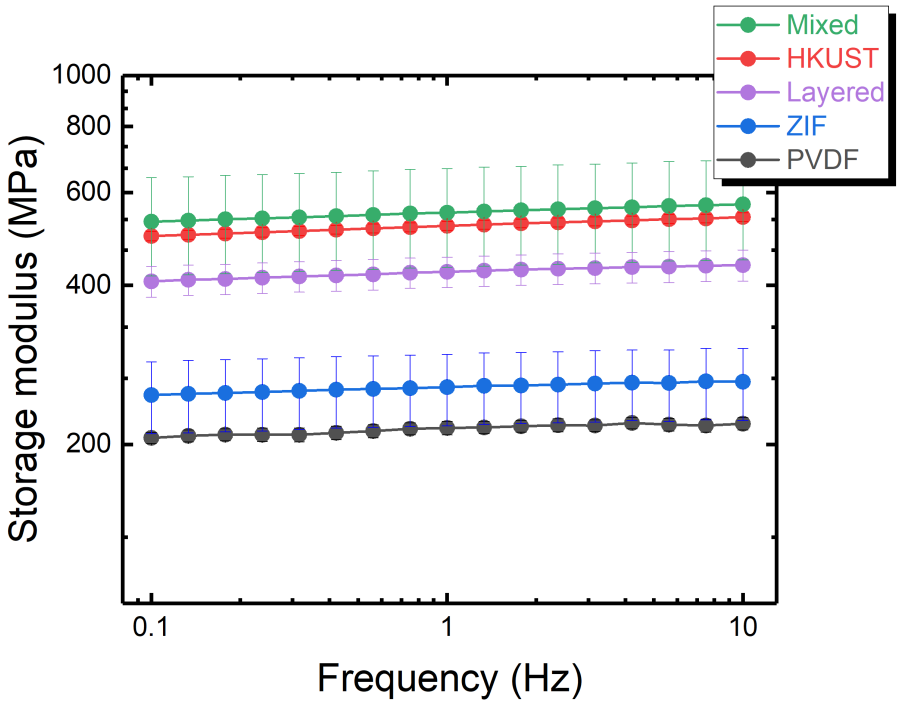

Figure S20. Storage modulus, *E*', as a function of frequency for MMM materials.

Table S1. Storage moduli at 1 Hz for MMM materials.

Sample	Modulus (MPa)
PVDF	215 ± 6
ZIF	257 ± 40
HKUST	519 ± 10
Mixed	549 ± 117
Layered	424 ± 28

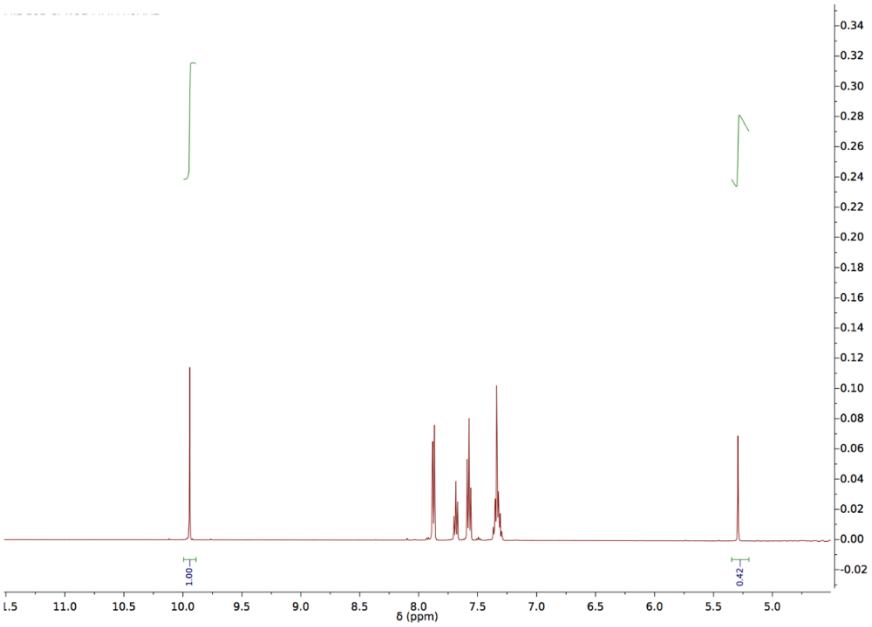

Figure S21. MIL-101-NO_2 MMM catalysis of benzaldehyde dimethyl acetal at 55 °C. The reaction shows 70% conversion of the starting material to benzaldehyde in the flow reactor.

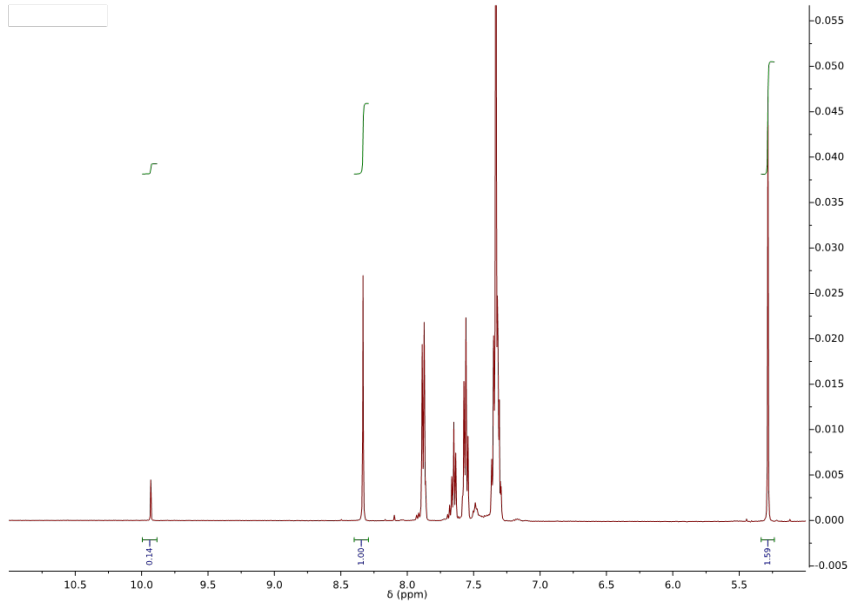

Figure S22. MIL-101-NO_2 MMM catalysis of benzaldehyde dimethylacetal at 55 °C with malonitrile in the reaction mixture. The reaction shows 42% conversion of the starting material to products in the flow reactor, with the majority of the intermediate benzaldehyde going on to react with malonitrile to form the final product. Of the products present, 12% is the benzaldehyde intermediate and 88% is the final product.

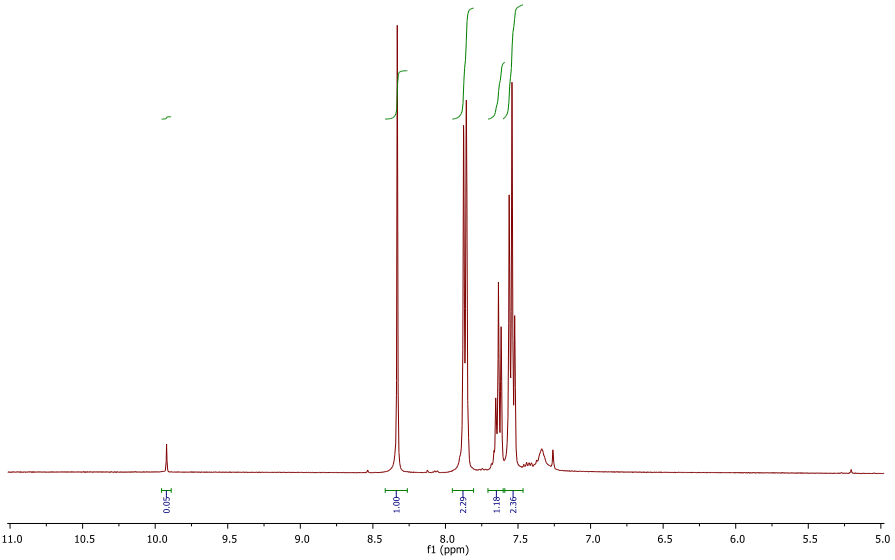

Figure S23. ZIF-8 MMM catalyzed Knoevenagel condensation at room temperature. ^{1}H NMR analysis of the eluent shows that 95% of the benzaldehyde successfully reacted with malonitrile, catalyzed by the ZIF-8 MMM at room temperature.

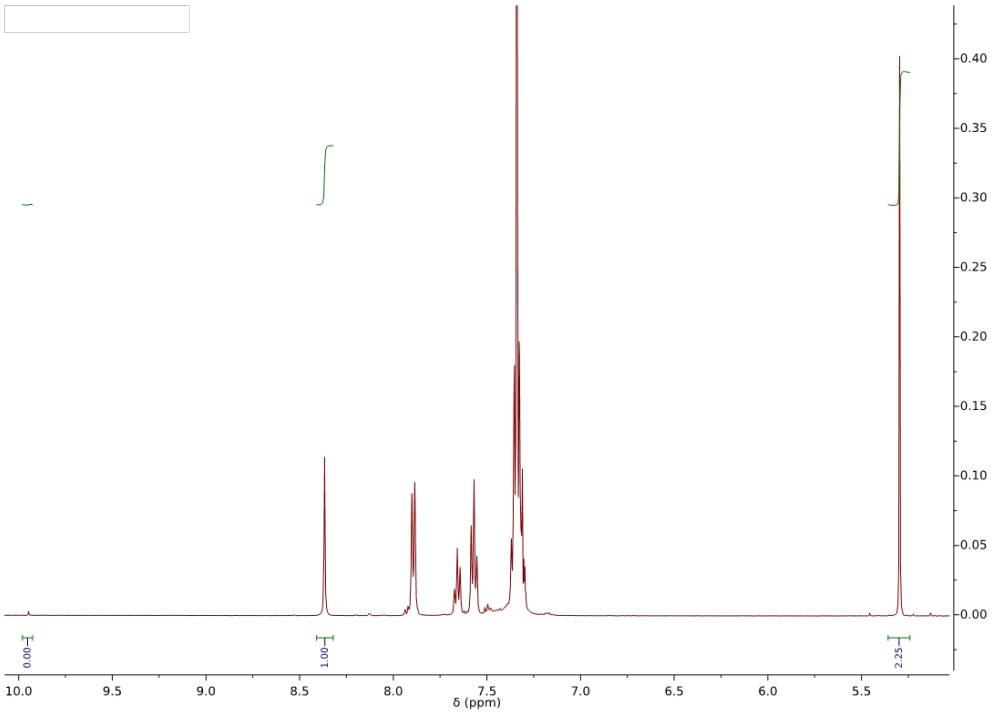

Figure S24. MIL-101-NO_2 and ZIF-8 mixed MMM catalyzed reactions at 55 °C. ^{1}H NMR analysis of the eluent shows that 31% of the starting material successfully reacted in the membrane reactor system. Of the products present, 99% is the final product over two steps in the membrane reactor, while only 1% remains as the benzaldehyde intermediate.

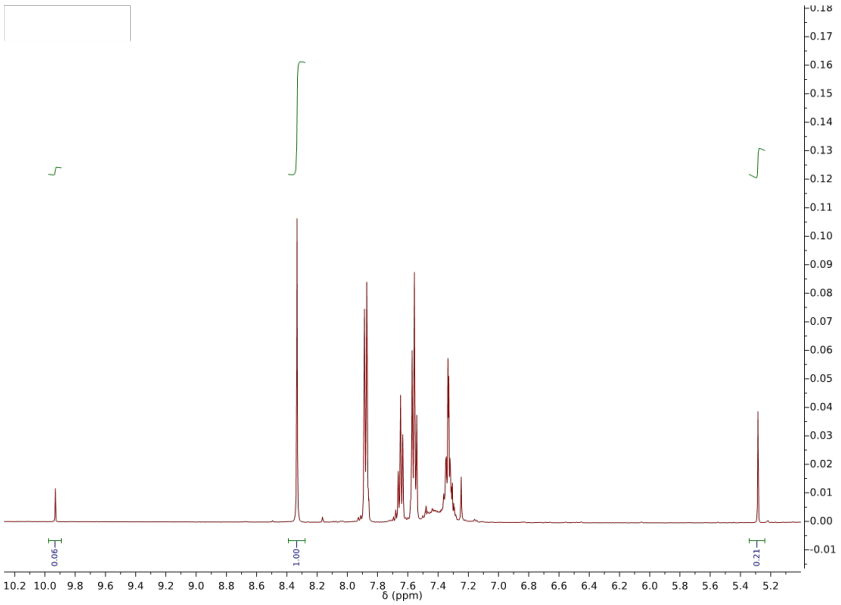

Figure S25. MIL-101-NO_2 and ZIF-8 layered MMM catalyzed reactions at 55 °C. ^{1}H NMR analysis of the eluent shows that 84% of the starting material successfully reacted in the membrane reactor system. Of the products present, 95% is the final product over two steps in the membrane reactor, while only 5% remains as the benzaldehyde intermediate.

References

(1) Cavka, J. H.; Jakobsen, S.; Olsbye, U.; Guillou, N.; Lamberti, C.; Bordiga, S.; Lillerud, K. P. *J. Am. Chem. Soc.* **2008**, *130*, 13850-13851.

(2) Zhuang, J.-L.; Ceglarek, D.; Pethuraj, S.; Terfort, A. *Adv. Func. Mater.* **2011**, *21*, 1442-1447.

(3) Venna, S. R.; Jasinski, J. B.; Carreon, M. A. *J. Am. Chem. Soc.* **2010**, *132*, 18030-18033.

(4) Taylor-Pashow, K. M.; Della Rocca, J.; Xie, Z.; Tran, S.; Lin, W. *J. Am. Chem. Soc.* **2009**, *131*, 14261-14263.

(5) Gordon, J.; Kazemian, H.; Rohani, S. *Microporous Mesoporous Mater.* **2012**, *162*, 36-43.

(6) Akiyama, G.; Matsuda, R.; Sato, H.; Hori, A.; Takata, M.; Kitagawa, S. *Micro. Meso Mater.* **2012**, *157*, 89-93.

(7) Denny, M. S., Jr.; Cohen, S. M. *Angew. Chem. Int. Ed.* **2015**, *54*, 9029-9032.

(8) Venna, S. R.; Lartey, M.; Li, T.; Spore, A.; Kumar, S.; Nulwala, H. B.; Luebke, D. R.; Rosi, N. L.; Albenze, E. *J. Mater. Chem. A* **2015**, *3*, 5014-5022.

(9) Basu, S.; Cano-Odena, A.; Vankelecom, I. F. J. *J. Membrane Sci.* **2010**, *362*, 478-487.